




Photoferroelectric phenomena in ferroelectric oxides and a Rayleigh analysis

Subhajit Pal, Atal Bihari Swain, Pranab Parimal Biswas , and Pattukkannu Murugavel ^{*}
Department of Physics, Indian Institute of Technology Madras, Chennai 600036, India

 (Received 21 November 2019; revised manuscript received 29 January 2020; accepted 5 June 2020; published 19 June 2020)

The recent renaissances in the field of ferroelectric oxides are owing to various photoinduced phenomena. However, the microscopic correlations among various photoinduced physical characteristics are essential for a detailed understanding of the dynamics associated with these phenomena. In this work, the photoinduced dielectric, pyroelectric, and ferroelectric properties of a lead-free $\text{Ba}_{0.875}(\text{Bi}_{0.5}\text{Li}_{0.5})_{0.125}\text{TiO}_3$ ferroelectric oxide are carried out in out-of-plane and in-plane geometry. The dielectric studies under 405-nm light illumination revealed a significant change in dielectric permittivity along with a decrease in Curie temperature. The observed effects are attributed to the change in internal field distribution inflicted by the photogenerated nonequilibrium charge carriers and trapped charges. The sample exhibits a photoinduced significant change in pyroelectric current and the associated polarization. These effects demonstrate that light could be used as an additional degree of freedom to influence the ferroelectric order parameter. The observed photoinduced dielectric and ferroelectric characteristics give the experimental evidence for the theoretical formalism on the photoinduced ferroelectric phenomena. In addition, the Rayleigh analysis performed on this system highlights the strong correlation between the observed photoferroelectric characteristics with the Rayleigh parameters. These findings could widen the understanding of the photoferroelectric characteristics to extend its applications toward advanced optoelectronic devices.

DOI: [10.1103/PhysRevMaterials.4.064415](https://doi.org/10.1103/PhysRevMaterials.4.064415)

I. INTRODUCTION

The interaction of light with ferroelectric systems led to several fascinating physical phenomena such as anomalous photovoltaic, photostriction, and photorefractive effects [1–5]. In recent times, the change in physical characteristics of the noncentrosymmetric ferroelectric system under the influence of light, called the photoferroelectricity, has attracted renewed interest [6–11]. This is due to its new application perspective in the optronics fields such as photoinduced random access memory devices, piezophototronic devices, photosensitive actuators, self-powered photodetectors, photovoltaic devices, photoinduced microsensing, microactuator, photostrictive-magnetostrictive magnetometers, light control gas storage applications, etc. [12–16]. The photoferroelectric (ph-FE) phenomenon is a cumulative effect of light on structural, dielectric, ferroelectric, and optical properties along with the interplay among them [7]. Thus, the microscopic mechanisms responsible for the ph-FE phenomenon are essential to envisage its application potential.

Earlier, several mechanisms such as Frank-Condon coupling, the pseudo-John-Teller optical center, the Glass model, and the Fridkin model were proposed to explain the ph-FE phenomenon [7,17]. Among them, the refined model proposed by Fridkin classified the ph-FE effect into two groups. The first group belongs to the ferroelectric system in the absence of an internal field, where the light-induced effects are correlated to the excitation of nonequilibrium carriers and the recharging

of levels. However, the second group belongs to the classic ferroelectrics in the presence of an internal field, where the light-induced effects are associated with an additional factor due to the resultant change in screening conditions. These factors affect both the magnitude and distribution of the internal field in the ferroelectric system and thereby modify the Curie temperature (T_C) as well as the ferroelectric properties [7]. Computational and experimental studies revealed that the internal field in the ferroelectrics is affected by several factors such as the electron transfer, hybridization of orbitals, spectral weight of electron density, defect centers, trap fillings, surface charges near the electrode-ferroelectric interface, etc. [18–20]. For example, the photogenerated charge carriers in BaTiO_3 are described to alter the $2p$ electron orbitals and thereby enhances the electronic polarization along the ionic polarization direction [8,20]. Alternatively, the photoinduced polarization reduction in HoMn_2O_5 system is attributed to the electronic polarization, which is opposite in direction to the ionic polarization [21]. In addition, photostriction in ferroelectric oxides is correlated to the converse piezoelectric effect originated from the photoinduced polarization change [22,23]. Although theoretical models are formulated for these photoinduced phenomena, the experimental evidence is lacking in the literature [7,20–23]. Also, the Rayleigh analysis usually performed on few piezoelectric systems showing enhanced properties near their morphotropic phase boundaries is not being carried out with respect to the photoinduced ferroelectric effect. The analysis corroborates the enhanced piezoelectric properties to the intrinsic and extrinsic parameters [24]. The intrinsic parameter is referred to as a change in ferroelectric properties caused by the lattice deformation and reversible domain-wall

^{*}muruga@iitm.ac.in

motion. On the other hand, the extrinsic Rayleigh parameter refers to the change in ferroelectric properties caused by irreversible domain-wall and phase boundary motions [25,26]. In this context, the Rayleigh analysis could be extended as a tool to understand the microscopic mechanism in the ph-FE effect.

For this purpose, the ph-FE studies are carried out on the recently reported lead-free $\text{Ba}_{0.875}(\text{Bi}_{0.5}\text{Li}_{0.5})_{0.125}\text{TiO}_3$ (BBLT) compound, where a giant photovoltaic response is demonstrated [27]. The photoinduced dielectric, pyroelectric, and ferroelectric characteristics studies revealed significant changes in their properties with a nearly 100% rise in polarization. The observed photoinduced effect is corroborated with the reported theoretical models. The microscopic changes observed in the BBLT sample are analyzed based on the extracted Rayleigh parameters. A strong correlation between the Rayleigh parameters and ph-FE characteristics is demonstrated in this work.

II. EXPERIMENTAL DETAILS

The BBLT compound was synthesized by a conventional solid-state reaction method using stoichiometric mixtures of analytical reagent-grade BaCO_3 (99.9%), Bi_2O_3 (99.9%), Li_2CO_3 (99.9%), and TiO_2 (99.9%) powders. The mixed oxide powder was calcined at 700°C for 4 h, followed by the second calcination at 800°C for 6 h. The final calcined powder was mixed with 6 wt. % polyvinyl alcohol as a binder and made into 8- and 12-mm-diameter green pellets. The green pellets were sintered at 1000°C for 2 h, and the density of the pellet was 96% of the theoretical value.

The x-ray diffraction (XRD) experiment was carried out by the Rigaku x-ray diffractometer using $\text{Cu-K}\alpha$ radiation for the structural information. To extract the optical band gap, a diffused reflectance spectroscopy experiment was performed using the ultraviolet-visible-near infrared (Jasco V-650) spectrophotometer. The ph-FE measurements were performed on 12-mm-diameter and 0.2-mm-thick sintered pellets in out-of-plane and in-plane geometries. For out-of-plane measurements, 0.5-mm-diameter Ag dots are used as top electrodes with Ag coating as a bottom electrode. For in-plane measurements, Ag strips of 1.0×0.2 mm dimension with 0.2 mm separation are used as electrodes. The top electrode was deposited by thermal evaporation technique at 10^{-5} mbar pressure, and the thickness of the electrode determined from Bruker Contour GT-3D surface profilometry was 32 nm. The ph-FE measurements were carried out by employing a 405-nm diode laser (model no. PSU-III-LED) as a light source. The temperature-dependent dielectric spectroscopy measurements were performed using PSM-1735 (NumericQ) LCR meter at various frequencies under dark and light conditions. Pyroelectric measurements were executed using a closed-cycle cryostat (Advance Research System) and Keithley electrometer (6517B). The measurements were carried out during the warming cycle at a rate of 5 K/min. Before the pyroelectric measurements, the sample was heated to 390 K and cooled down to 300 K under the poling field of ± 20 kV/cm. The polarization measurements were carried out using a Radiant Technology (USA RT6000S) loop tracer at 300 K.

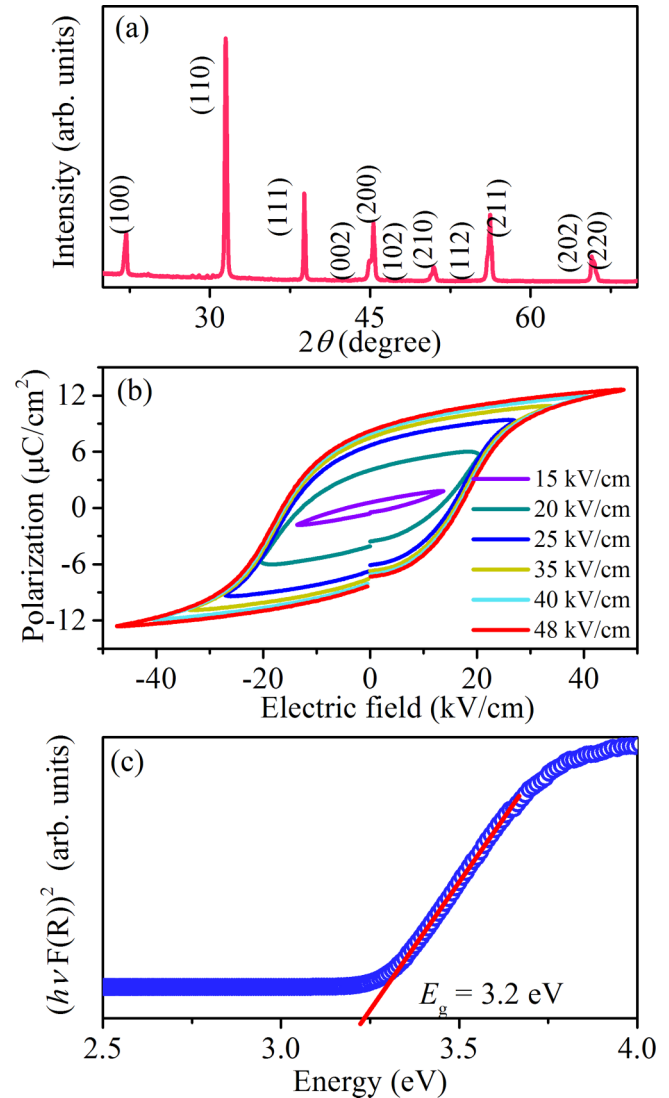


FIG. 1. (a) The XRD pattern, (b) the polarization vs electric fields measured at 4 Hz, and (c) the Kubelka-Munk plot of the BBLT sample.

III. RESULTS AND DISCUSSION

A. Structural, ferroelectric, and optical properties

The XRD pattern recorded on the BBLT sample at 300 K is shown in Fig. 1(a). The pattern reveals that the compound is formed in pure phase without any trace of impurities, and the pattern is indexed to tetragonal crystal symmetry with a $P4mm$ space group. To ascertain the ferroelectric characteristic, the polarization (P) versus electric field (E) is measured at 4 Hz at various maximum electric fields. The obtained P - E hysteresis loops shown in Fig. 1(b) reveal that the remnant polarization (P_r) of the BBLT sample is $8.19 \mu\text{C}/\text{cm}^2$. The evolution of the P - E loops and its well-saturated hysteretic character at high applied field confirm the ferroelectric nature of the sample without any leakage behavior. To determine the optical band gap, the diffuse reflectance spectrum is recorded on the sample. The respective $[F(R)h\nu]^2$ plotted against $h\nu$ is shown in Fig. 1(c), where $F(R) = \frac{(1-R)^2}{2R}$ is the

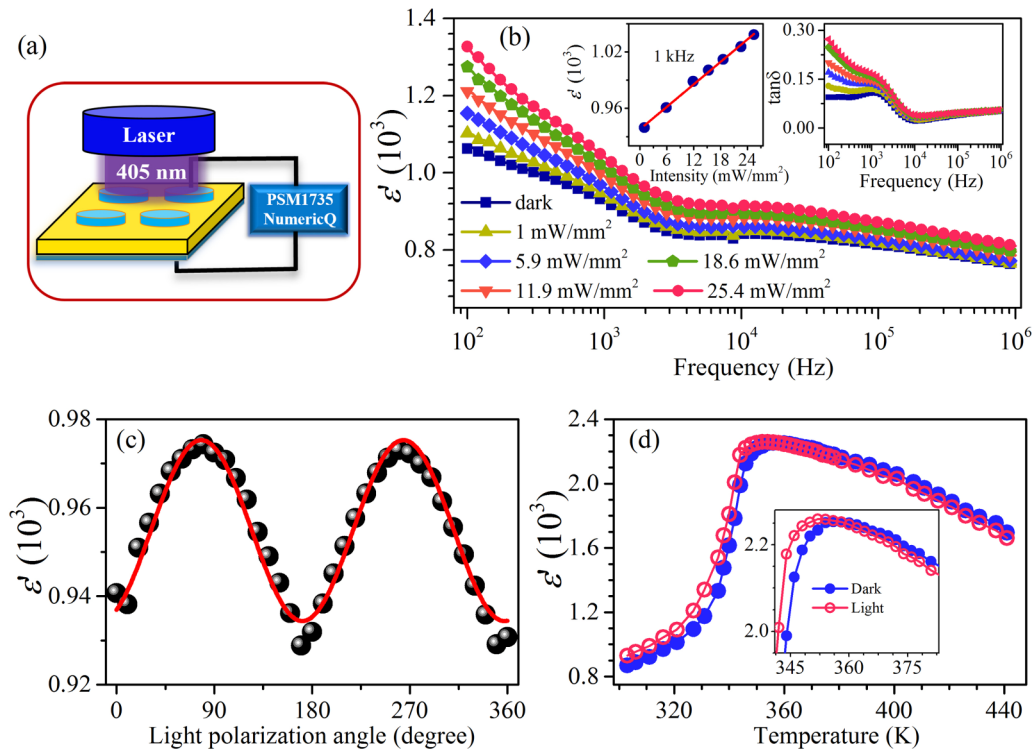


FIG. 2. (a) Schematic representation of the experimental setup used for dielectric measurements. (b) Frequency variation of ϵ' under different light intensities for the BBLT sample. The left inset shows an intensity variation of ϵ' and right inset shows frequency variation of dielectric loss ($\tan\delta$) with different light intensities. (c) Light polarization angle-dependent ϵ' measured using linear polarized light (11.9 mW/mm^2). The solid symbol and solid line represent the experimental and calculated data points, respectively. (d) Temperature-dependent ϵ' measured at 1 kHz under dark and 11.9 mW/mm^2 light illumination conditions. Inset shows a zoomed version of the figure.

Kubelka-Munk function, R is the reflectance, h is the Planck's constant, and ν is the frequency [28,29]. The band gap extracted from the plot is 3.2 eV.

B. Photoinduced dielectric and ferroelectric characteristics

To investigate the photoinduced effect, the frequency-dependent dielectric measurement is performed from 100 Hz to 1 MHz under dark and light illumination conditions at 300 K on an unpoled BBLT sample in the out-of-plane geometry. Figure 2(a) shows the schematic representation of the experimental setup used for dielectric measurements. The real part of dielectric permittivity (ϵ') recorded as a function of frequency at various light intensities is plotted in Fig. 2(b). The plots reveal an evident photoinduced variation in ϵ' with respect to the light intensities. The larger dispersion seen at low-frequency range could be attributed to the dominant light-induced space charge contribution over the other dielectric contributions [30]. The variation of ϵ' measured under dark, and the maximum light intensity (25.4 mW/mm^2) at 100 Hz is $\sim 20\%$, and it decreases to 9% at 10 kHz. The change in ϵ' observed even at a higher frequency range eliminates several resistive and capacitive mechanisms such as space-charge depletion regions, interfacial accumulation mechanisms, etc. [31]. To elucidate it further, the frequency-dependent dielectric loss tangent ($\tan\delta$) at various light intensities is plotted in the right side inset of Fig. 2(b). The negligible dispersion in $\tan\delta$ seen at high-frequency regions illustrates that the observed photoinduced dielectric response is indeed intrinsic

in nature. Generally, ϵ' is found to obey the power-law dependency concerning light intensity [32]. Consequently, the ϵ' shows a linear variation with the light intensity as revealed by the intensity-dependent ϵ' drawn at 1 kHz shown in the left inset of Fig. 2(b).

The light polarization direction-dependent photocurrent density [33] and photodeformation [4] effects are studied on a few ferroelectric systems. Hence, the photoinduced dielectric response in the BBLT sample could also show the light polarization direction-dependent features. This is indeed tested by measuring ϵ' in usual capacitor geometry at a various incident light polarization angle, which is varied along the in-plane direction of the sample under 11.9 mW/mm^2 light condition. The resultant data plotted in Fig. 2(c) shows a sinusoidal angular dependence of the photoinduced dielectric response with the light polarization direction. The ϵ' shows the maximum variation of $\sim 20\%$ between 0° and 90° light polarization angle at 1 kHz frequency. The reported similar features in light polarization direction-dependent photocurrent density, and photodeformation studies strongly suggest the correlation among these phenomena [4,33]. Since ϵ' is primarily influenced by the light illumination at room temperature, the temperature-dependent ϵ' is measured to study the photoinduced phase transition. The ϵ' measured at 1 kHz under dark and 11.9 mW/mm^2 light illumination are shown in Fig. 2(d). Interestingly, the photogenerated nonequilibrium carriers in the BBLT sample influence the symmetry breaking paraelectric to ferroelectric phase transition (T_C), and hence facilitate the transition to happen at a lower temperature. The

inset shown in Fig. 2(d) reveals that the T_C is reduced by 4 K after light illumination. Normally, the ferroelectric systems exhibit structural instabilities driven by factors such as electric field, temperature, and pressure [2,27,34]. The observed photo-induced change in T_C ascertains that light can be a factor for influencing the structural instabilities. Such a light-induced phase transition can be understood by the proposed theoretical model in the literature. In ferroelectric phase transition studies, the electron-subsystem contribution to the total free energy is generally overlooked due to its insulating characteristics. However, the carrier concentration in a ferroelectric oxide can be increased by several extrinsic factors, including the photogenerated carriers. In such ferroelectric oxides, the electron-subsystem contribution cannot be neglected while performing the free-energy calculation. Consequently, the free energy is the sum of the lattice contributions in the paraelectric and ferroelectric region along with electron-subsystem contribution. Therefore, the net free energy $F = F_0 + F_1 + F_2$, where F_0 and F_1 are free energies of the lattice in paraelectric and ferroelectric regions, respectively. F_2 is the free energy of electron subsystem. Overall, the free-energy expression of a ferroelectric system under light can be expressed by [7,12]

$$\begin{aligned}
 F(T, P, \sigma_k, N) = & F_{0N} + \frac{1}{2}\alpha_N P^2 + \frac{1}{4}\beta_N P^4 + \frac{1}{6}\gamma_N P^6 \\
 & + N \sum_k \ddot{E}'_k \sigma_k - \frac{1}{2} \sum_i \sum_k S_{Nik} \sigma_i \sigma_k \\
 & - P^2 \sum_k v_{Nk} \sigma_k. \quad (1)
 \end{aligned}$$

Here α , β , and γ are coefficients in the free-energy expression, N is the energy level with a free-electron concentration n . The other coefficients are defined as $F_{0N} = F_0 + N\ddot{E}_0$, $\alpha_N = \alpha + aN$, $\beta_N = \beta + bN$, $\gamma_N = \gamma + cN$, where \ddot{E}_0 corresponds to energy in the paraelectric state. a , b , and c are constants representing the second-, fourth-, and sixth-order partial derivative of total energy with respect to polarization near the phase-transition temperature. Also, $v_{Nk} = v_k - \ddot{E}_k''' N$, $S_{Nik} = S_{ik} - \ddot{E}_{ik}'' N$, and σ_k are the components of electrostriction, elastic constant, and mechanical stress tensor. \ddot{E}'_k , \ddot{E}_{ik}'' , and \ddot{E}_{ik}''' are the first-, second-, and third-order partial derivatives of energy term with respect to mechanical stress tensor elements, respectively [7,12]. Overall, the free energy given in Eq. (1) is comprised of two equations of state. The first one yields the generated electric field ($E = \frac{dF}{dP}$) in the system, and the second one is the component of deformation tensor ($u_k = -\frac{dF}{d\sigma_k}$) due to photoinduced effects. Hence, the ferroelectric system under the light will experience a change in free energy due to photoinduced excitation of nonequilibrium charge carriers. Therefore, materials under light illumination are expected to go through additional variation in their physical quantities such as T_C , P , and lattice deformation. Consequently, the photoinduced change in T_C is given by $\Delta T_C = T_{CN} - T_C = -\frac{C}{2\pi} aN$, where C is the Curie-Weiss constant, T_{CN} , and T_C are the Curie points with and without light. The minimum free energy condition gives $a > 0$, and hence the effect of photoinduced charge carriers is expected to lower the T_C [7,35]. In case of parent BaTiO₃, the theoretical estimation of the ΔT_C is -3.8 K after considering the values of $C = 3 \times 10^5$ K, $a = 0.8 \times 10^{-23}$, and $N = 10^{19}/\text{cm}^3$ [36]. Note

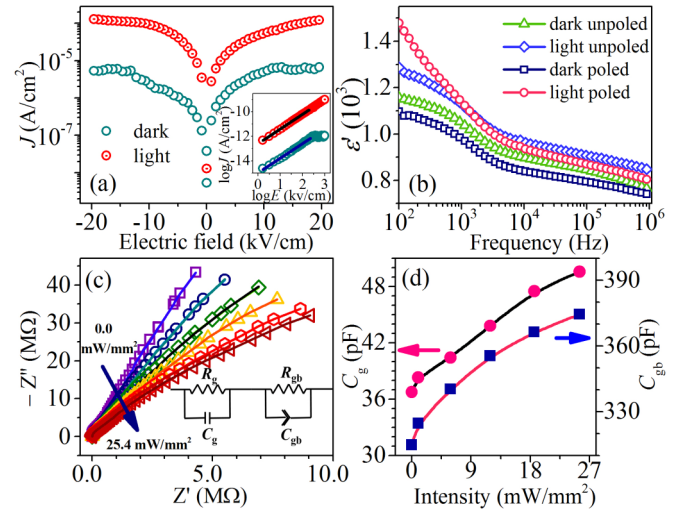


FIG. 3. (a) J - E curve measured under dark and light conditions. The inset is the respective $\log(J)$ vs $\log(E)$ plots. (b) Frequency-dependent ϵ' measured under dark and 11.9-mW/mm² light in poled and unpoled conditions. (c) $-Z''$ vs Z' plots measured under dark and various light intensities. The inset shows the equivalent R - C circuits used to fit the data. The open symbols and solid lines represent the experimental and fitted data. (d) Variation of grain and grain-boundary capacitance under dark and various light intensities.

that the experimental observation for the ΔT_C for the BBLT system is -4 K, which is close to the theoretical value of parent compound [7,36]. The experimental observation shown in Fig. 2(d) is in accordance with the reported theoretical model and thereby gives experimental evidence for the same [7].

The photoinduced effects on ϵ' and ΔT_C could be attributed to various mechanisms associated with the free charges, trapped charges, surface charges near electrodes, alteration of Schottky barrier height, and Poole-Frenkel conduction [7,37]. To elucidate their roles in the observed dielectric characteristics in the BBLT system, the leakage current density (J), frequency-dependent ϵ' under poled and unpoled states, and impedance studies are carried out at dark and light illumination conditions. To understand the free and trapped charges contributions, J versus E curves recorded under dark and light conditions are shown in Fig. 3(a). Under dark, the J - E curve displays a saturation at a higher field, which indicates the absence of free and trapped charge contributions to the conduction mechanism. On the contrary, upon light illumination (11.9 mW/mm²), the J - E curve reveals an increase in current even up to the maximum applied field (20 kV/cm). This is considered an indication for the photoinduced free and trapped charge contributions to the conduction mechanism. Note that trapping centers present in the sample facilitate the effective collection of photogenerated charge carriers by trapping one of the charge carriers (positive or negative) and thereby avoiding their recombination. This can be further verified from the slope of the $\log(J)$ versus $\log(E)$ plot, whose value is expected to be ~ 1 and >1 for the trap-free and a trapped charge related conduction mechanism, respectively [8,37]. The corresponding $\log(J)$ versus $\log(E)$ plots shown as an inset in Fig. 3(a) reveal that the values of the slopes under

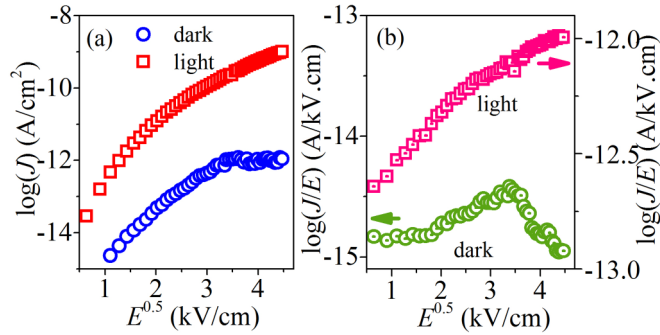


FIG. 4. (a) $\log(J)$ vs $E^{0.5}$ and (b) $\log(J/E)$ vs $E^{0.5}$ plots.

dark is 1.05 and under light is 1.24. These values reiterate the free and trapped charge contributions to the photoinduced conduction mechanisms [8].

To probe the effect of surface charge contributions, the ϵ' is measured under dark and light in both poled and unpoled conditions and the resultant plots are shown in Fig. 3(b). Note that upon poling, the surface charge distribution near the electrode-ferroelectric interface could be altered due to the screening effect [7]. From Fig. 3(b), it is inferred that the % change in ϵ' ($\Delta\epsilon'$) observed between dark and light at the low-frequency region in the poled condition is higher (34% at 100 Hz) in comparison with the respective value in unpoled (11% at 100 Hz) condition, whereas, in the high-frequency region, the respective $\Delta\epsilon'$ show only subtle difference in values between poled (9.3% at 10 kHz) and unpoled (7.8% at 10 kHz) condition. These features elucidate that the surface charge contributions to ϵ' dominate only at low frequency.

To probe it further, the real (Z') and imaginary (Z'') parts of the impedance are measured on the sample from 100 Hz to 1 MHz at 300 K under dark and various light intensities. The respective $-Z''$ versus Z' plots are shown in Fig. 3(c). The plots are fitted with an equation representing the series combination of R - C equivalent circuits, displayed as an inset in Fig. 3(c). It is to be noted that the experimental data are best fitted with equivalent circuits representing only grain and grain-boundary contributions. This excludes the electrode interface related contribution, if any [38]. Additionally, the extracted grain (C_g) and grain-boundary capacitance (C_{gb}) values plotted in Fig. 3(d) display an increasing trend with light intensities. The increase in C_g and C_{gb} upon light intensity elucidate that the photoinduced change in ϵ' could be correlated to the generation of photoinduced charges and trapped charges across the grains and grain boundaries [39]. Note that these charge carriers can influence the piezoelectric tensor elements and thereby causes the deformation in the sample [22,23].

The effect of other possible sources such as alteration of Schottky barrier height and the Pool-Frenkel conduction can be analyzed based on the leakage current response to the applied electric field. From the Schottky emission model, the $\log(J)$ is expected to show a linear variation with $E^{0.5}$. Similarly, according to the Poole-Frenkel conduction model, the $\log(J/E)$ is expected to show a linear variation with $E^{0.5}$. In contrast, the respective plots shown in Figs. 4(a) and 4(b) under dark and light conditions reveal only the nonlinear char-

acteristics behaviors. Hence, the observed features exclude Schottky emission and Pool-Frenkel conduction contributions to the photoinduced dielectric response [37].

Similar to the change in dielectric properties of the materials, the spontaneous polarization of a ferroelectric system under light can be derived from the free-energy expression as

$$P_{0N}^2 = P_0^2 \left[1 + \frac{bN}{\beta} - \frac{cN}{\gamma} \right], \quad (2)$$

where P_0 and P_{0N} are the polarization before and after light illumination, respectively [7]. Also, the deformation under the light in a piezoelectric crystal can be expressed as

$$u_{kN} = u_k \left[1 + \frac{\Delta P_{0N}^2}{P_0^2} - \frac{\ddot{E}_k'''}{v_k} \right] - N \ddot{E}_k' \quad (3)$$

where $u_k = v_k P_0^2$, $\Delta P_{0N}^2 = (P_{0N} - P_0)^2$

Equation (3) advocates the correlation between the photoinduced polarization and lattice deformation parameters [7]. However, experimental evidence for such correlations is not reported. In this work, the BBLT ceramics have been subjected to the pyroelectric and ferroelectric polarization measurements under light to explore such correlation. The pyroelectric current is measured from 300 to 390 K under dark and 11.9-mW/mm² light conditions. The measurements are carried out on a sample for positive and negative poled states. The observed plots are displayed in Fig. 5(a). The pyroelectric current shows a photoinduced effect at all temperatures below T_C (~ 351 K). Above T_C , the plots revealed negligible variation in photocurrent, which rules out the contribution from the photoconduction, if any, in the BBLT sample. The polarization values are extracted from the observed pyroelectric current using $P = \frac{1}{A\beta} \int i dT$ relation, where A , i , β , and dT are the surface area, pyroelectric current, heating rate, and change in temperature of the sample, respectively [40]. The obtained polarization values under negative and positive poled conditions are plotted in Fig. 5(b). The figure confirms the ph-FE effect where the BBLT sample exhibits a significant change in polarization in both positive and negative poled states at 300 K. From the phenomenological theory on BaTiO₃ by Devonshire, the estimated values of P_0 , β , b , and c near phase transition temperature are 2.3×10^2 cgs units, 2.7×10^{-13} cgs units, 2.6×10^{-33} , and 0, respectively [7,36]. The relative change in polarization ($\Delta P_{0N}/P_0$) for the BaTiO₃ compound calculated from Eq. (3) is $\sim 3.7 \times 10^{-2}$. However, the $\Delta P_{0N}/P_0$ for the BBLT sample observed near the phase-transition temperature shown in Fig. 5(b) is $\sim 3.5 \times 10^{-1}$ which is an order of magnitude higher than the BaTiO₃. This could be due to the superior photovoltaic characteristics of the BBLT sample and the consequent better ph-FE properties in comparison to the parent compound [27].

To ascertain it further, the P - E hysteresis measurements are repeated under light illumination on the BBLT sample up to 40 kV/cm field and 300 K temperature. The P - E loops recorded at 4 Hz under dark, 1.0-, 5.9-, and 11.9-mW/mm² light intensities are plotted in Fig. 5(c). The figure reveals the $2P_r$ values of 14.6, 15.9, 20.6, and 29.4 $\mu\text{C}/\text{cm}^2$ under dark, 1.0, 5.9, and 11.9 mW/mm² light intensities. Remarkably, the BBLT sample displays the maximum change in polarization

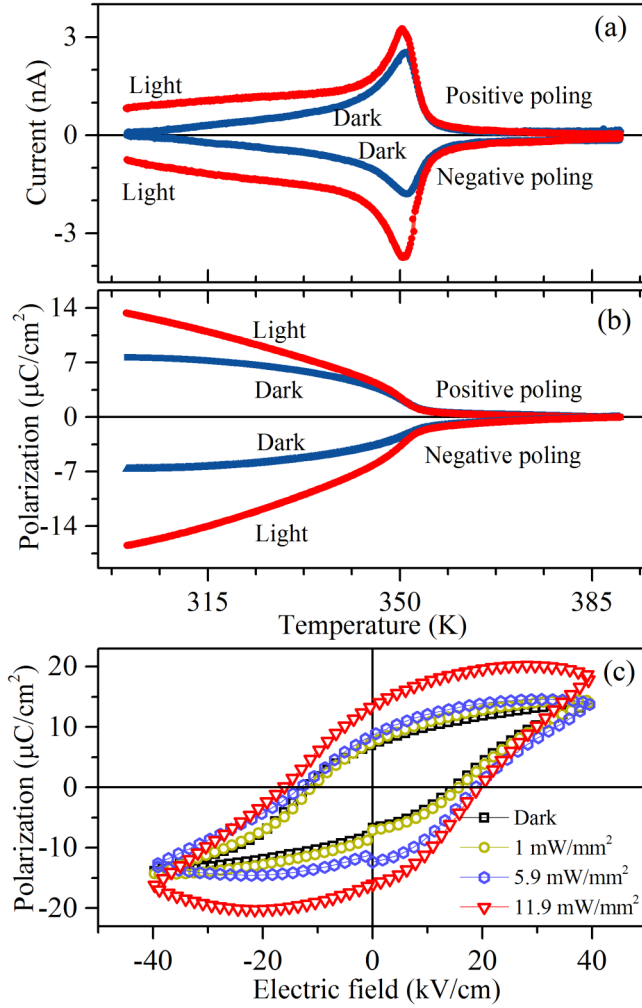


FIG. 5. (a) Temperature-dependent pyroelectric current measured under dark and 11.9-mW/mm² light conditions on positive and negative poled BBLT sample. (b) The respective temperature-dependent polarization plots extracted from the pyroelectric current measurements. (c) P - E loops measured under 1.0-, 5.9-, and 11.9-mW/mm² light intensities at 300 K and 4 Hz.

under 11.9-mW/mm² light intensity, which reconfirms the ph-FE effect observed from the pyroelectric measurements.

C. Photoferroelectric phenomena in electrically homogeneous medium

It is to be noted that the thickness of the sample under study is larger than the light penetration depth. Consequently, the sample could be electrically inhomogeneous in the out-of-plane direction under the light illumination condition. However, the sample can be considered as electrically homogeneous along the in-plane direction under light illumination. To understand the photoinduced effect in an electrically homogeneous medium in comparison to the inhomogeneous medium, the measurements are repeated in in-plane geometry, as shown by the schematic diagram in Fig. 6(a). Here, the electrode separation distance (0.2 mm) is lower than the laser beam diameter (1.5 mm) but the same as the sample thickness. The frequency-dependent ϵ' and $\tan\delta$

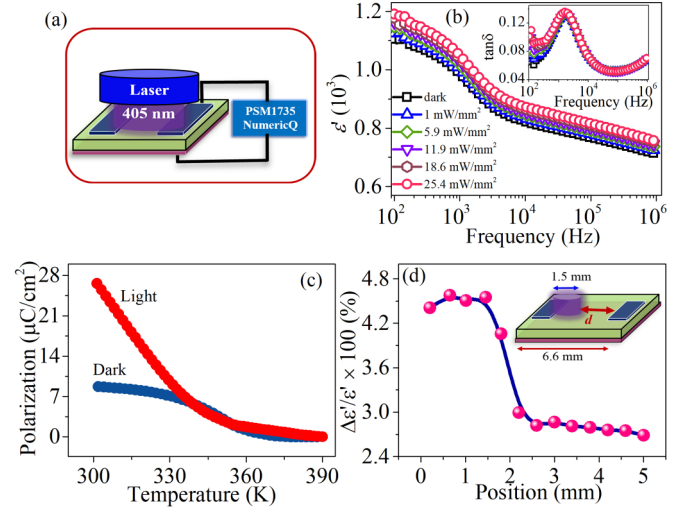


FIG. 6. (a) Schematic representation of the experimental setup used for in-plane electrical measurements. (b) Frequency variation of ϵ' under different light intensities for the BBLT sample. The inset shows a frequency variation of $\tan\delta$ with light intensities. (c) Temperature-dependent polarization plots extracted from the pyroelectric current measurements on the positive poled BBLT sample under dark and light conditions. (d) ϵ' measured as a function of electrode separation distance under 11.9-mW/mm² light intensity. The inset shows the schematic of the measurement setup.

recorded under various light intensities are plotted in Fig. 6(b) and the inset of Fig. 6(b), respectively. The change in ϵ' under dark and maximum light intensity (25.4 mW/mm²) at 100 Hz is $\sim 7.9\%$, and it decreases to 4.5% at 10 kHz. Also, the $\tan\delta$ shows negligible variation at higher frequency range (> 1 kHz range). The temperature-dependent ferroelectric polarization obtained from the pyroelectric current measurements under dark and 11.9 mW/mm² light conditions are shown in Fig. 6(c). The observed features displayed by ϵ' , $\tan\delta$, and polarization are similar to the results observed in electrically inhomogeneous conditions. However, other surface related contributions to the light-induced phenomenon reported on the centrosymmetric SrTiO₃ (100) crystal are not completely ruled out in the in-plane measurement geometry [41].

Additionally, to verify the effect of electrical inhomogeneity, the ϵ' measurement is repeated in in-plane geometry at various electrode separation distance (d) varied from 0.2 to 5 mm in steps of 0.2 mm, as shown in the schematic diagram displayed in the inset of Fig. 6(d). The respective percentage change in ϵ' ($\frac{\Delta\epsilon'}{\epsilon'} \times 100$) measured at 10 kHz and 11.9 mW/mm² is shown in Fig. 6(d), where $\Delta\epsilon'$ is the difference in ϵ' with respect to the dark and light conditions. The plot shows that $\frac{\Delta\epsilon'}{\epsilon'} \times 100$ remains at 4.5% up to $d < 2$ mm followed by a sharp drop to 2.7% beyond $d > 2$ mm. The drop in $\frac{\Delta\epsilon'}{\epsilon'} \times 100$ for $d > 2$ mm, i.e., beyond the laser illuminated area, is due to the effect of an additional dielectric layer where the contribution from the photoinduced effect is absent. Although the presence of electrical inhomogeneity in the sample, in terms of the layers with and without photoinduced effect, lowers the $\frac{\Delta\epsilon'}{\epsilon'} \times 100$ value, the observed 2.7% change in dielectric constant reiterates the general pho-

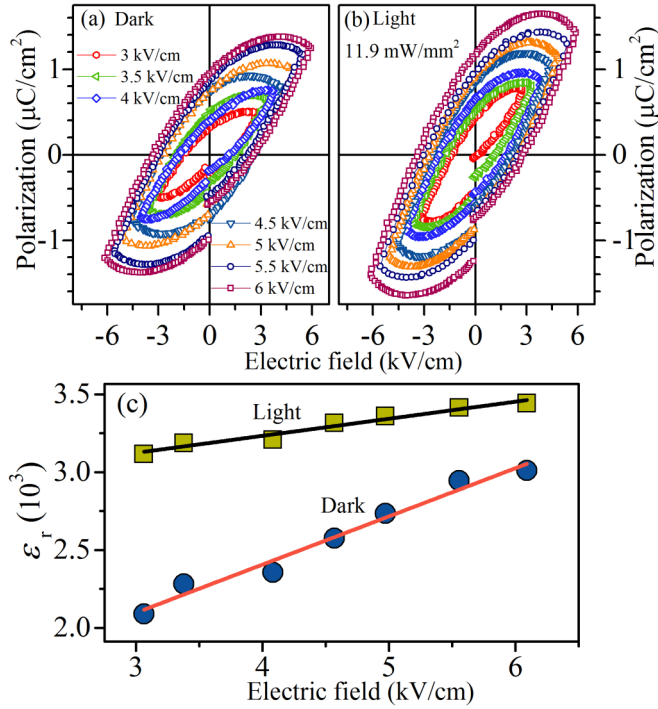


FIG. 7. Low-field P - E hysteresis measurements under (a) dark and (b) light (11.9 mW/mm^2) conditions. (c) The changes in dielectric coefficient ϵ_r as a function of an electric field for dark and light conditions.

photoinduced phenomenon displayed by the ferroelectric BBLT sample.

D. Effect of light on the Rayleigh analysis

The dielectric and ferroelectric properties influenced by the photoinduced effects are examined by the Rayleigh equation ($\epsilon_r = \epsilon_{\text{int}} + \alpha E_0$) containing the intrinsic and extrinsic parameters, where ϵ_r is the dielectric coefficient, ϵ_{int} is the intrinsic Rayleigh parameter, α is the coefficient of the extrinsic Rayleigh parameter, and E_0 is the applied electric-field amplitude [42]. The ϵ_{int} is related to lattice deformation and reversible domain-wall motion. On the other hand, the coefficient α describes the irreversible domain-wall motion of the system [25]. To perform the Rayleigh analysis, ϵ_r is calculated from the expression $\epsilon_r = \frac{P_{p-p}}{2E_0}$, where P_{p-p} , the peak-to-peak polarization, corresponds to an applied E_0 value [43]. For this purpose, the P - E measurements under the light are carried out at various electric fields (3 – 6 kV/cm) below the subcoercive field region. The measured P - E hysteresis loops under dark and 11.9-mW/mm^2 light intensity are plotted in Figs. 7(a) and 7(b), respectively. The P_{p-p} values observed in Figs. 7(a) and 7(b) at various E_0 are used to calculate ϵ_r , and it is displayed in Fig. 7(c). The observed linear variation of ϵ_r with E_0 confirms the validity of the Rayleigh approach. Furthermore, to extract the intrinsic and the extrinsic parameters, the ϵ_r versus E_0 plots are fitted with the Rayleigh equation. The fitting reveals that the ϵ_{int} is increased from 2035 to 3100, and α is decreased from 1.78 to 0.9 mm/V under the light. The enhanced value of ϵ_{int} upon

light illumination is attributed to the photoinduced lattice deformation and reversible domain-wall motion. Additionally, the observed reduction in α under light illustrates the influence of photoinduced effects on the irreversible domain-wall motion.

In general, the decrease in α is associated with a decrease in the domain-wall mobility which in turn is expected to decrease ϵ' . However, the dielectric response has both intrinsic and extrinsic contributions. The fraction of the extrinsic contribution to the measured dielectric response is given by $f_\alpha = \frac{\epsilon_{\text{ext}}}{\epsilon_{\text{int}} + \epsilon_{\text{ext}}} = \frac{\alpha E_0}{\epsilon_{\text{int}} + \alpha E_0}$ [26]. In the present case, the calculated extrinsic contribution to the dielectric response is about 52% for dark and 14% for light illumination conditions. This indicates that under light illumination, the intrinsic parameter (the observed lattice deformation and reversible domain-wall motion) is dominating over the extrinsic one (irreversible domain-wall motion). Hence, the ϵ' follows an increasing trend, which is in accordance with the dominant intrinsic contributions.

The observed photoinduced effects on polarization and dielectric response, as seen in Figs. 5 and 2, is directly correlated to the photoinduced lattice deformation expressed in Eq. (3), where the deformation is proportional to $\frac{\Delta P_{0N}^2}{P_0^2}$. The origin for such lattice deformation could come from the photogenerated nonequilibrium charges and trapped charges, as mentioned earlier. Although the exact deformation of lattice in the ferroelectric oxide is to be estimated from the photostriction measurement, the present study gives a correlation between photoinduced change in ferroelectric properties and lattice deformation.

IV. CONCLUSIONS

In conclusion, BBLT exhibits photoinduced effects with a substantial change in dielectric and ferroelectric properties upon 405-nm light illumination. The observed photoinduced effects on the dielectric response and the ferroelectric polarization are attributed to the photogenerated nonequilibrium charge carriers and trapped charges in the BBLT system. The experimentally observed photoinduced change in Curie temperature ($\Delta T_C \sim 4 \text{ K}$) and the relative change in polarization ($\Delta P_{0N}/P_0 \sim 3.5 \times 10^{-1}$) are in accordance with the theoretical formalism. The $\Delta P_{0N}/P_0$ value being an order of magnitude higher compared to the parent BaTiO_3 (3.7×10^{-2}) illustrates the superior ph-FE properties of the BBLT sample. Interestingly, the demonstrated light polarization direction-dependent dielectric behavior and the photoinduced increment in the intrinsic Rayleigh parameter suggests that the ph-FE phenomena can be correlated to the photodeformation effect and reversible domain-wall motion. Overall, these studies elucidate further insight into the ph-FE phenomena along with the possibilities of integrating the photoinduced effects in the ferroelectric system into the existing optoelectronic devices.

ACKNOWLEDGMENTS

Authors acknowledge Prof. M. S. Ramachandra Rao, Dr. M. Rath, and S. Pradhan for P - E loop measurements.

- [1] B. I. Sturman and V. M. Fridkin, *The Photovoltaic and Photorefractive Effects in Noncentrosymmetric Materials* (Gordon and Breach Science, Philadelphia, 1992).
- [2] A. B. Swain, D. Murali, B. R. K. Nanda, and P. Murugavel, *Phys. Rev. Appl.* **11**, 044007 (2019).
- [3] A. B. Swain, M. Rath, P. P. Biswas, M. S. R. Rao, and P. Murugavel, *APL Mater.* **7**, 011106 (2019).
- [4] B. Kundys, M. Viret, D. Colson, and D. O. Kundys, *Nat. Mater.* **9**, 803 (2010).
- [5] P. Gunter and J. P. Huignard, *Photorefractive Materials and Their Applications 2: Materials* (Springer, New York, 2005).
- [6] A. S. Makhort, F. Chevrier, D. Kundys, B. Doudin, and B. Kundys, *Phys. Rev. Mater.* **2**, 012401(R) (2018).
- [7] V. M. Fridkin, *Photoferroelectrics* (Springer-Verlag, Berlin, 1979).
- [8] H. Borkar, V. Rao, M. Tomar, V. Gupta, J. F. Scott, and A. Kumar, *RSC Adv.* **7**, 12842 (2017).
- [9] H. Borkar, M. Tomar, V. Gupta, R. S. Katiyar, J. F. Scott, and A. Kumar, *Mater. Res. Express* **4**, 086402 (2017).
- [10] J. Kreisel, M. Alexe, and P. A. Thomas, *Nat. Mater.* **11**, 260 (2012).
- [11] Y. Bai, G. Vats, J. Seidel, H. Jantunen, and J. Juuti, *Adv. Mater.* **30**, 1803821 (2018).
- [12] K. Uchino, *Ferroelectric Devices* (Marcel Dekker, New York, 2000).
- [13] Y. Dai, C. Wu, Z. Wu, Z. Zhao, L. Li, Y. Lu, and Z. L. Wang, *Adv. Sci.* **6**, 1900314 (2019).
- [14] B. Kundys, *Appl. Phys. Rev.* **2**, 011301 (2015).
- [15] J. K. Li, C. Ge, K. J. Jin, J. Du, J. Yang, H. Lu, and G. Yang, *Appl. Phys. Lett.* **110**, 142901 (2017).
- [16] J. E. Spanier, V. M. Fridkin, A. M. Rappe, A. R. Akbashev, A. Polemi, Y. Qi, Z. Gu, S. M. Young, C. J. Hawley, D. Imbrenda, G. Xiao, A. L. B. Jackson, and C. L. Johnson, *Nat. Photon.* **10**, 611 (2016).
- [17] G. Chanussot, *Ferroelectrics* **20**, 37 (1978).
- [18] C. Paillard, E. Torun, L. Wirtz, J. Iniguez, and L. Bellaiche, *Phys. Rev. Lett.* **123**, 087601 (2019).
- [19] P. Wang, J. Zhao, L. Wei, Q. Zhu, S. Xie, J. Liu, X. Meng, and J. Li, *Nanoscale* **9**, 3806 (2017).
- [20] S. M. Young and A. M. Rappe, *Phys. Rev. Lett.* **109**, 116601 (2012).
- [21] G. Giovannetti and J. van den Brink, *Phys. Rev. Lett.* **100**, 227603 (2008).
- [22] C. Paillard, S. Prosandeev, and L. Bellaiche, *Phys. Rev. B* **96**, 045205 (2017).
- [23] C. Paillard, B. Xu, B. Dkhil, G. Geneste, and L. Bellaiche, *Phys. Rev. Lett.* **116**, 247401 (2016).
- [24] J. Gao, Y. Wang, Y. Liu, X. Hu, X. Ke, L. Zhong, Y. He, and X. Ren, *Sci. Rep.* **7**, 40916 (2017).
- [25] J. Gao, X. Hu, L. Zhang, F. Li, L. Zhang, Y. Wang, Y. Hao, L. Zhong, and X. Ren, *Appl. Phys. Lett.* **104**, 252909 (2014).
- [26] M. Abebe, K. Brajesh, and R. Ranjan, *J. Appl. Phys.* **122**, 034101 (2017).
- [27] S. Pal, A. B. Swain, P. P. Biswas, D. Murali, A. Pal, B. R. K. Nanda, and P. Murugavel, *Sci. Rep.* **8**, 8005 (2018).
- [28] H. S. Kim, C. R. Lee, J. H. Im, K. B. Lee, T. Moehl, A. Marchioro, S. J. Moon, R. H. Baker, J. H. Yum, J. E. Moser, M. Gratzel, and N. G. Park, *Sci. Rep.* **2**, 591 (2012).
- [29] H. Bai and X. Liu, *Mater. Lett.* **100**, 1 (2013).
- [30] E. J. J. Perez, R. S. Sanchez, L. Badia, G. G. Belmonte, Y. S. Kang, I. M. Sero, and J. Bisquert, *J. Phys. Chem. Lett.* **5**, 2390 (2014).
- [31] O. Almora, C. Aranda, and G. G. Belmonte, *J. Phys. Chem. C* **122**, 13450 (2018).
- [32] M. M. A. Gader, K. A. Wishah, Y. A. Mahmud, M. A. H. Abdallah, and R. N. A. Bitar, *Appl. Phys. A* **43**, 123 (1987).
- [33] A. Bhatnagar, A. R. Chaudhuri, Y. H. Kim, D. Hesse, and M. Alexe, *Nat. Commun.* **4**, 2835 (2013).
- [34] P. E. Janolin, P. Bouvier, J. Kreisel, P. A. Thomas, I. A. Kornev, L. Bellaiche, W. Crichton, M. Hanfland, and B. Dkhil, *Phys. Rev. Lett.* **101**, 237601 (2008).
- [35] H. Borkar, V. Rao, S. Dutta, A. Barvat, P. Pal, M. Tomar, V. Gupta, J. F. Scott, and A. Kumar, *J. Phys.: Condens. Matter* **28**, 265901 (2016).
- [36] M. E. Drougard, R. Landauer, and D. R. Young, *Phys. Rev.* **98**, 1010 (1955).
- [37] D. Lee, S. H. Baek, T. H. Kim, J. G. Yoon, C. M. Folkman, C. B. Eom, and T. W. Noh, *Phys. Rev. B* **84**, 125305 (2011).
- [38] J. C. G. Abrantes, J. A. Labrincha, and J. R. Frade, *Mater. Res. Bull.* **35**, 727 (2000).
- [39] S. Nandy, P. S. V. Mocherla, and C. Sudakar, *J. Appl. Phys.* **121**, 203102 (2017).
- [40] E. J. Sharp and L. E. Garn, *J. Appl. Phys.* **53**, 8980 (1982).
- [41] E. Meirzadeh, D. V. Christensen, E. Makagon, H. Cohen, I. R. Goldian, E. H. Morales, A. Bhowmik, J. M. G. Lastra, A. M. Rappe, D. Ehre, M. Lahav, N. Pryds, and I. Lubomirsky, *Adv. Mater.* **31**, 1904733 (2019).
- [42] M. Abebe, K. Brajesh, J. S. Malhotra, and R. Ranjan, *J. Phys. D: Appl. Phys.* **51**, 185601 (2018).
- [43] R. E. Eitel, T. R. Shrout, and C. A. Randall, *J. Appl. Phys.* **99**, 124110 (2006).